



## RBF-DQ Solution of Natural Convection under the Effect of a Magnetic Field in a Tilted Cavity

B. Pekmen Geridönmez

*Basic Sciences Unit, TED University, Ziya Gokalp Caddesi, No.48, 06420, Kolej-Cankaya, Ankara, Turkey*

*Email: bengisenpekmen@gmail.com*

(Received August 1, 2016; accepted October 24, 2016)

### ABSTRACT

In this study, radial basis function based differential quadrature (RBF-DQ) method is applied to the natural convection in an inclined unit square cavity under the effect of an applied magnetic field in different angles. The stream function-vorticity form of the dimensionless governing equations are concentrated on. The change in different Hartmann numbers, Rayleigh numbers and inclination angles of the cavity is investigated both in terms of streamlines, isotherms, vorticity contours and the average Nusselt number through the heated wall. The increase in Hartmann number causes heat transfer to be conductive due to the Lorentz force, and therefore the inclination angle of the cavity loses its effect. A remarkable effect of the inclination angle on heat transfer for  $10^4 \leq Ra \leq 10^6$  is presented. The proposed method is a global method and provides to use small number of grid points as a result of DQ method.

**Keywords:** Radial basis functions; Differential quadrature method; Natural convection; Tilted cavity.

### 1. INTRODUCTION

Natural convective heat transfer under the effect of a magnetic field in closed enclosures has received intense curiosity due to the extensive applications in crystal growth process, solar technologies, nuclear reactors, micro electronic devices, food and metallurgical industries etc. In most of the studies, differentially heated horizontal or vertical walls are examined. Inclined walls have also taken attention due to the effects on heat transfer and fluid flow by tangential and normal components of buoyancy force.

Different numerical techniques in different geometries are applied to simulate natural convection in differentially heated enclosures. Cianfrini *et al.* (2005) numerically studied the natural convection in a tilted, differentially opposite heated walls in a cavity employing the SIMPLE algorithm. They found that the inclination angle around  $135^\circ$ , and  $315^\circ$  causes the overall heat transfer to be larger than  $0^\circ$  along the x-, and y-axes, respectively. Finite volume method (FVM) and SIMPLE algorithm is applied for simulation of the same problem involving a centered, conducting block by Das and Reddy (2006). The inclination angle between  $0^\circ$  and  $90^\circ$  has no effect at a low Ra value while the convective heat transfer increases with the increase in the angle. Pirmohammadi and

Ghassemi (2002) take into account the presence of a magnetic field in an inclined cavity. Using the SIMPLE algorithm which is based on finite volume code, they showed that convective heat transfer strongly depends on the angle between  $0^\circ$  and  $135^\circ$  for  $Ra = 10^4$  and  $Ra = 10^5$ . Control volume based SIMPLER algorithm is also used by Han (2009) to simulate natural convection in a tilted cavity including electrically conducting fluid. The influence of the inclination angle on the electromagnetic retarding force is emphasized while the effect of inclination angle disregarded with the increase in the magnitude of the applied magnetic field. Lacerda and Colaço (2014) have examined the magneto convection in a tilted cavity using RBF approximation. They solved the governing equations only in stream function (biharmonic) and temperature equation. Lattice Boltzmann method (LBM) is applied in Munir *et al.* (2011) to this problem in different types of boundary conditions. Up to an inclination angle, average Nusselt number is higher in case of adiabatic boundary conditions than the case of perfectly boundary conditions. The same method is also carried out by Huelsz and Rechtman (2013) to discuss the same problem. Hysteresis depending on Rayleigh number is noticed. Basak *et al.* (2014) have analyzed the inclination angle utilizing the Galerkin finite element method with a penalty parameter. Their results demonstrated that convective heat transfer is pronounced at  $15^\circ$  and  $30^\circ$  at a high  $Pr = 998$ . A finite

volume Navier-Stokes solver in combination with Adams-Bashforth for nonlinear terms and Crank-Nicolson for the viscous and diffusion terms is used by Williamson *et al.* (2016) as  $Ra = 10^4 - 10^8$  and  $Pr = 7$ . A critical angle where a bifurcation occurs in the flow is found. In this case, transient and single mode flow is noted while the multi-nodal flow takes place with the increase in the angle. Kherief *et al.* (2016) considered the natural convection problem in presence of magnetic field in an inclined rectangular cavity applying the finite volume method. The formation of counter-rotating eddies in the counterclockwise inclination is reported. The same conclusion is also encountered by Kherief *et al.* (2012) by using the same method in the MHD natural convection problem in a cavity filled with mercury.

Natural convection in an inclined cavity in 3D is also investigated in some studies. Lo *et al.* (2007) and Ravnik *et al.* (2008) applied DQ method and boundary element method (BEM), respectively, to this problem in velocity-vorticity form of the equations. They found that Nusselt number decreases at each Rayleigh number as the inclination angle increases from  $0^\circ$  to  $60^\circ$ . In both study, the usage of considerably small number grid points ( $25^3$ ) is noted.

Radial basis function (RBF) based method have taken great deal of interest in the last decade. RBFs provide independence from mesh, and therefore they become indispensable for meshless free methods. The novel books by Buhmann (2003) and Fasshauer (2007) involve many details and applications about RBFs.

Having high accuracy, differential quadrature (DQ) method discretizes the derivatives by weighting coefficients using all grid points in the domain. This method is firstly introduced by Bellman *et al.* (1972), and the concise basics on the method are presented by Shu (2000).

The combination of DQ and RBFs is studied in some studies. Shu *et al.* (2004) showed the efficiency of RBF based-DQ applying the method to linear and nonlinear examples. They showed that considerably small number of grid points with arbitrary distribution result in good accuracy. To enable one to obtain well-conditioned matrices when the number of grid points are increased, an upwind local RBF based-DQ method is proposed by Shu *et al.* (2005). They applied this approach to inviscid compressible flows, and concluded that complex geometries can be managed by this method independently from the node generation. Integrated RBF based-DQ method is also investigated by Shu and Wu (2007). Better accuracy on Burger's equation and Navier-Stokes equations than RBF based-DQ is observed.

In the present study, natural convection in an inclined, differentially heated, unit square cavity under the effect of a magnetic field is investigated by using the RBF-DQ method. The objective of this study is to analyze the effect of both inclination angles in the enclosure and the applied magnetic field, and to examine the efficiency of the RBF-DQ

method using the small number of grid points.

## 2. MATHEMATICAL BASIS

The two-dimensional, unsteady, laminar flow of a Newtonian, incompressible, viscous fluid in a unit square cavity is considered. Viscous dissipation, Joule heating and radiation effect are neglected. The magnetic Reynolds number is assumed to be small so that the induced magnetic field can be neglected.

The physical properties of the fluid is constant except the density variation following from Boussinesq approximation which is  $\rho = \rho_0[1 - \beta(T - T_0)]$  with  $\beta = -(1/\rho)[\partial\rho/\partial T]_p$ , and subindex 0 refers to reference state.

The governing equations with continuity equation, momentum equations and energy equation in terms of the velocity  $\mathbf{u} = \langle u, v \rangle$ , pressure  $p$  and temperature  $T$  are written as

$$\nabla \cdot \mathbf{u} = 0 \tag{1a}$$

$$v \nabla^2 u = \frac{\partial u}{\partial t} + u \frac{\partial u}{\partial x} + v \frac{\partial u}{\partial y} + \frac{1}{\rho} \frac{\partial p}{\partial y} - \frac{\sigma B_0^2}{\rho} (v \sin \theta \cos \theta - u \sin^2 \theta) + g_x \beta (T - T_c) \sin \theta \tag{1b}$$

$$v \nabla^2 v = \frac{\partial v}{\partial t} + u \frac{\partial v}{\partial x} + v \frac{\partial v}{\partial y} + \frac{1}{\rho} \frac{\partial p}{\partial x} - \frac{\sigma B_0^2}{\rho} (u \sin \theta \cos \theta - v \cos^2 \theta) + g_y \beta (T - T_c) \cos \theta \tag{1c}$$

$$\alpha \nabla^2 T = \frac{\partial T}{\partial t} + \mathbf{u} \cdot \nabla T, \tag{1d}$$

where  $\nu$  is the kinematic viscosity,  $\rho$  is the density of the fluid,  $\sigma$  is the electrical conductivity of the fluid,  $B_0$  is the magnitude of the applied magnetic field,  $\theta$  is the inclination angle of the applied magnetic field,  $\varphi$  is the inclination angle of the enclosure,  $g_x$  and  $g_y$  are  $x$  and  $y$  components of the gravitational acceleration  $g$ ,  $\beta$  is the thermal expansion coefficient, and  $\alpha$  is the thermal diffusivity.

In order to obtain dimensionless equations, the following non-dimensional variables are defined as

$$x' = \frac{x}{L}, \quad y' = \frac{y}{L}, \quad u' = \frac{ul}{\alpha}, \quad v' = \frac{vl}{\alpha}, \tag{2}$$

$$p' = \frac{\rho L^2}{\rho \alpha^2}, \quad t' = \frac{t \alpha}{L^2}, \quad T' = \frac{T - T_c}{T_h - T_c}, \tag{3}$$

where  $L$  is the characteristic length.

These dimensionless variables are substituted into Eq. (1). Then, the prime notation is dropped, and  $u - v - p - T$  form of non-dimensional equations are obtained. In order not to tackle with pressure terms, the stream function  $\psi$  is defined as

$\partial\Psi/\partial y = u$ ,  $\partial\Psi/\partial x = -v$  satisfying the continuity equation. Vorticity equation is obtained by taking difference of the derivative of momentum equations as  $\partial v/\partial x - \partial u/\partial y$  which is the definition of vorticity.

The dimensionless governing equations in terms of stream function  $\psi$ , temperature  $T$  and vorticity  $w$  are deduced as

$$\nabla^2\Psi = -w \quad (4a)$$

$$\nabla^2 T = \frac{\partial T}{\partial t} + u \frac{\partial T}{\partial x} + v \frac{\partial T}{\partial y} \quad (4b)$$

$$\begin{aligned} \nabla^2 w = & \frac{1}{Pr} \left( \frac{\partial w}{\partial t} + u \frac{\partial w}{\partial x} + v \frac{\partial w}{\partial y} \right) \\ & - Ra \left( \frac{\partial T}{\partial x} \cos\phi - \frac{\partial T}{\partial y} \sin\phi \right) \\ & - Ha^2 \left( \frac{\partial u}{\partial y} \sin^2\theta - 2 \frac{\partial v}{\partial y} \sin\theta \cos\theta - \frac{\partial v}{\partial x} \cos^2\theta \right). \end{aligned} \quad (4c)$$

Dimensionless parameters resulting from the non-dimensionalization are

$$Pr = \frac{\nu}{\alpha}, \quad Ra = \frac{g\beta(T_h - T_c)L^3}{\alpha\nu}, \quad Ha = B_0L\sqrt{\frac{\sigma}{\rho\nu}}, \quad (5)$$

Prandtl, Rayleigh and Hartmann numbers, respectively.

Problem geometry is described in Fig. 1. The walls with  $T_h$  and  $T_c$  are heated and cold walls, respectively, and the jagged walls are adiabatic walls. On each walls,  $u = v = \Psi = 0$ . The magnitude of the applied magnetic field is  $|\mathbf{B}| = B_0$ . Vorticity boundary conditions are unknown.

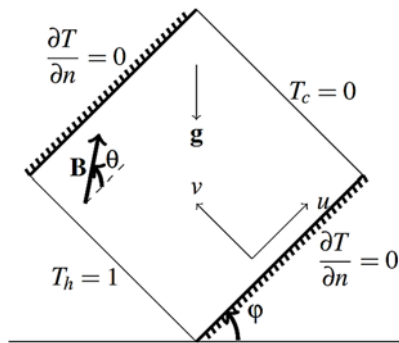


Fig. 1. Problem Configuration.

### 3. RBF-DQ METHOD AND ITS APPLICATION

DQ method approximates the derivatives of a function by a linear weighted sum of all functional values in the whole physical domain.

For a two-dimensional problem, the partial derivatives of a function  $g$  are approximated by DQ method as (Shu 2000)

$$g_x(x_k, y_k) = \sum_{\ell=1}^{NM} \xi_{k\ell} f(x_\ell, y_\ell) \quad (6)$$

$$g_y(x_k, y_k) = \sum_{\ell=1}^{NM} \bar{\xi}_{k\ell} f(x_\ell, y_\ell), \quad (7)$$

where  $N, M$  are the number of grid points, and  $\xi_{k\ell}$  and  $\bar{\xi}_{k\ell}$  are the weighting coefficients in  $x$  and  $y$  directions, respectively.

RBF methods approximate a function  $g$  using a radial basis function  $\chi$  as

$$g_i = \sum_{\ell=1}^{NM} c_j \chi_{ij}, \quad (8)$$

where  $c_j$ 's are coefficients to be determined,  $i = 1, \dots, NM$  refers to index of any field point in the domain.  $\chi_j$  is a function of radial distance  $r = r = \|\mathbf{x} - \mathbf{x}_j\|_2$  in which  $\mathbf{x} = (x, y)$  is a field point and  $\mathbf{x}_j = (x_j, y_j)$  is a collocation point.

In matrix-vector form, Eq. (8) can be written as

$$g = Fc, \quad (9)$$

where  $F$  is the matrix of size  $NM \times NM$  formed by  $\chi_{ij}$ 's columnwise.

Equivalently, Eq. (9) can be rewritten as

$$c = F^{-1}g. \quad (10)$$

Any derivative of  $g$  may also be expressed as in Eq. (9) using Eq. (10), i.e.

$$\frac{\partial g}{\partial x} = \frac{\partial F}{\partial x} c = \frac{\partial F}{\partial x} F^{-1} g, \quad \text{or} \quad \frac{\partial g}{\partial y} = \frac{\partial F}{\partial y} c = \frac{\partial F}{\partial y} F^{-1} g. \quad (11)$$

By means of DQ method,  $n^{th}$  order partial derivatives of  $g$  may also be written in matrix-vector form as

$$\frac{\partial^n g}{\partial x^n}(x_k, x_k) = \sum_{\ell=1}^{NM} \xi_{k\ell}^{(n)} g(x_\ell, y_\ell) = \xi^n g \quad (12)$$

$$\frac{\partial^n g}{\partial x^n}(x_k, x_k) = \sum_{\ell=1}^{NM} \bar{\xi}_{k\ell}^{(n)} g(x_\ell, y_\ell) = \bar{\xi}^n g, \quad (13)$$

where  $\xi^n$  and  $\bar{\xi}^n$  are matrices of size  $NM \times NM$  formed by the weighting coefficients.

From Eq. (11), we can also derive  $n$ th order partial derivative by RBF method for any point  $(x_k, y_k)$  as

$$\frac{\partial^n g}{\partial x^n} = \frac{\partial^n F}{\partial x^n} F^{-1} g, \quad \frac{\partial^n g}{\partial y^n} = \frac{\partial^n F}{\partial y^n} F^{-1} g. \quad (14)$$

Thus, the weighting coefficients  $\xi^n$  and  $\bar{\xi}^n$  of RBF-DQ method in Eqs. (12) and (13) are obtained

using Eq. (14) as

$$\xi^n = \frac{\partial^n F}{\partial x^n} F^{-1}, \quad \bar{\xi}^n = \frac{\partial^n F}{\partial y^n} F^{-1}. \quad (15)$$

As an application of RBF-DQ method to the described problem in this study, once the space derivatives are discretized by RBF-DQ and employing the Backward Euler time integration scheme for the time derivatives, the iterative system on the dimensionless governing equations are constructed as follows

$$D_2 \Psi^{m+1} = -w^m \quad (16a)$$

$$u^{m+1} = D_y \Psi^{m+1}, \quad v^{m+1} = -D_x \Psi^{m+1} \quad (16b)$$

$$\left( D_2 - \frac{1}{\Delta t} - M \right) T^{m+1} = -\frac{T^m}{\Delta t} \quad (16c)$$

$$\left( D_2 - \frac{1}{Pr\Delta t} - \frac{M}{Pr} \right) w^{m+1} = -\frac{w^m}{Pr\Delta t} - Ra(\cos\theta D_x T^{m+1} - \sin\theta D_y T^{m+1}) - Ha^2(\sin^2\theta D_y u^{m+1} - 2\sin\theta\cos\theta D_y v^{m+1} - \cos^2\theta D_x v^{m+1}) \quad (16d)$$

where  $D_2$  is the Laplacian matrix formed by second order weighting coefficients of RBF-DQ as

$$D_2 = \frac{\partial^2 F}{\partial x^2} F^{-1} + \frac{\partial^2 F}{\partial y^2} F^{-1}, \quad D_x \text{ and } D_y \text{ are first order}$$

weighting coefficients of RBF-DQ as  $D_x = \frac{\partial F}{\partial x} F^{-1}$

and  $D_y = \frac{\partial F}{\partial y} F^{-1}$ ,  $M = [u]_d^{m+1} D_x + [v]_d^{m+1} D_y$ ,  $I$

matrix of size  $NM \times NM$ , and  $m$  shows the iteration.

The unknown vorticity boundary conditions are easily handled by

$$w = \frac{\partial v}{\partial x} - \frac{\partial u}{\partial y} = D_x v^{m+1} - D_y u^{m+1}. \quad (17)$$

The sequential iteration starts with the initial values of  $\psi$ ,  $w$ ,  $T$  which are taken as zero except on boundary. After solving Eq. (16a), velocity components are computed by Eq. (16b). The boundary conditions for  $u$ ,  $v$  are inserted. Then,  $u$ ,  $v$  are used in  $M$  matrix, and also in the computation of vorticity boundary conditions.

The criterion to stop the iterations is as follows (Khanafer *et al.* 1999)

$$\frac{\|\Psi^{m+1} - \Psi^m\|_\infty}{\|\Psi^m\|_\infty} + \frac{\|T^{m+1} - T^m\|_\infty}{\|T^m\|_\infty} + \frac{\|w^{m+1} - w^m\|_\infty}{\|w^m\|_\infty} < \varepsilon, \quad (18)$$

in which  $\varepsilon=10^{-5}$  is the tolerance. Satisfaction of Eq. (18) means that the steady-state is reached.

The Dirichlet type boundary conditions are inserted into the system matrix directly. The Neumann boundary conditions are added to the system matrix

which results in an overdetermined system. The systems of the form  $Ax = b$  are solved by Gaussian elimination with partial pivoting, and QR factorization is carried out for overdetermined system.

Multiquadric (MQ) RBF  $f = \sqrt{r^2 + c^2}$  is chosen in this study.  $c$  is called the ‘shape parameter’ which controls the shape of the basis functions. As  $c$  gets larger, the shape becomes flat and the matrix becomes more ill-conditioned.

MQ collocation matrices are conditionally positive definite (Fasshauer (2007); Michelli (1986)). Also, the exponential convergence of the error of MQ approximation have been demonstrated by Madych and Nelson (1992).

The convenient shape parameter  $c$  is determined by an idea similar to LOOCV (leave one out of cross validation).

- An interval of  $c$ , for which the well-conditioned system matrices are provided, is taken firstly. The interval is divided into equal  $c$  values.
- At any  $c_i$  value, average Nusselt number through the heated wall  $\overline{Nu}$  is computed with  $NM$  and  $NM - 1$  number of grid points.
- The value of  $c_i$  giving the result of the error  $\frac{\overline{Nu}^{NM} - \overline{Nu}^{NM-1}}{\overline{Nu}^{NM}}$  smallest, in which  $\overline{Nu}^{NM}$  and  $\overline{Nu}^{NM-1}$  are the average Nusselt numbers with  $NM$  and  $NM - 1$  grid points, is chosen, respectively.

Inverse matrices in Eq. (16) are managed by using right back slash operator in Matlab which is based on Gaussian elimination with partial pivoting. For instance,

$D_x = \frac{\partial F}{\partial x} F^{-1}$  is computed as

$$D_x = \frac{\partial F}{\partial x} / F \text{ while } D_x F = \frac{\partial F}{\partial x}.$$

The average Nusselt number through the heated left wall is defined by  $\overline{Nu} = \int_0^1 -\frac{\partial T}{\partial x} dy$ , and computed by

Clenshaw Curtis quadrature (Trefethen 2000) due to the usage of Chebyshev non-uniform grid distribution.

#### 4. NUMERICAL RESULTS

Prandtl number is fixed as  $Pr = 0.71$ . After finding the vorticity at  $(m + 1)^{th}$  time, a relaxation parameter is used as  $w^{m+1} \leftarrow \gamma w^{m+1} + (1 - \gamma)w^m$  for accelerating the convergence in which  $0 < \gamma < 1$ . Because, reaction terms in vorticity equation involve all parameters.

The proposed method is validated by the bench-mark problem in Davis (1983) comparing the average Nusselt number values through the heated wall. As can be seen from Table 1, the results with RBF-DQ

**Table 1 Comparison of  $\overline{Nu}$  through the left heated wall**

Present						
Ra	c	$\Delta t$	$\gamma$	Grids	$\overline{Nu}$	Davis(1983)
$10^3$	0.08	0.01	0.1	21×21	1.117	1.118
$10^4$	0.09	0.01	0.1	21×21	2.245	2.243
$10^5$	0.075	0.005	0.1	23×23	4.53	4.519
$10^6$	0.05	0.001	0.1	29×29	8.868	8.8

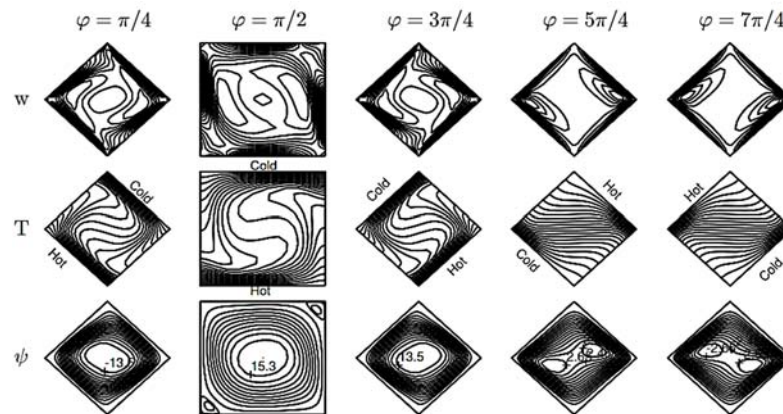


**Fig. 2. The angle  $\phi$  changes when  $Ra = 10^5$ ,  $Ha = 10$ ,  $\theta = 0$ .**

yield well agreement with the results in Davis (1983), in which the resolution is  $41 \times 41$ , using the small number of grid points. As  $Ra$  increases, the value of the shape parameter decreases, and instead of decreasing  $\gamma$ ,  $\Delta t$  is decreased.

Grid independence is presented for  $\phi = \pi/4$ ,  $\theta = 0$ ,  $Ra = 10^5$  in different  $Ha$  values in Table 2. Even

**Table 2 Grid independence**

Grids	$\overline{Nu}$		
	$Ha = 150$	$Ha = 50$	$Ha = 100$
2121	1.26	2.57	4.44
2323	1.25	2.55	4.43
2525	1.25	2.55	4.43
2727	1.25	2.54	4.42

if  $23 \times 23$  number of grid points are enough for  $Ha = 10$  and  $Ha = 50$ ,  $25 \times 25$  number of grid points are fixed for all  $Ha$  values unless otherwise declared.

In Fig. 2, the variation of the inclination angle  $\phi$  of the enclosure is depicted by vorticity contours, isotherms and streamlines from top row to bottom row. In case of  $\phi = \pi/4$  and  $\phi = 3\pi/4$ , symmetric behaviour is seen in each contours. Regarding the contour signs of streamlines, clockwise ( $\phi = \pi/4$ ) and counter-clockwise ( $\phi = 3\pi/4$ ) centered cells appear.  $\phi = \pi/2$  exhibits the Rayleigh-Benard convection with counterclockwise rotation in stream-lines. The

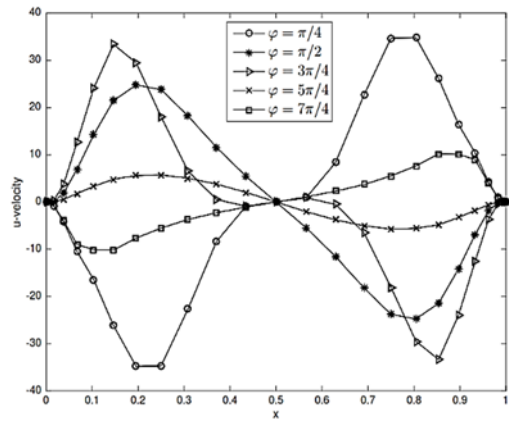
temperature gradient through the top and bottom walls is intensified in isotherms. With  $\phi = 5\pi/4$  and  $\phi = 7\pi/4$ , convective heat transfer is reduced as is seen from nearly orthogonal isotherms to the adiabatic walls. The main, centered cell in streamlines noted in  $\phi = \pi/4$ ,  $3\pi/4$  is divided into two cells in both  $\phi = 5\pi/4$  and  $\phi = 7\pi/4$  values.

Figure 3 demonstrates  $u$  and  $v$  velocity profiles along the line  $y=x$  in some angles  $\phi$  when  $Ra = 10^5$ ,  $Ha = 10$  are fixed.  $u$ -velocity increases up to  $x = y = 0.5$  at  $\phi = 3\pi/4$  and  $\phi = 5\pi/4$  while it decreases at  $\phi = \pi/4$  and  $\phi = 7\pi/4$ . From  $x = y = 0.5$  to  $x = y = 1$ , this state turns out, and  $u$ -velocity increases for  $\phi = \pi/4$  and  $\phi = 7\pi/4$ , while it decreases for  $\phi = 3\pi/4$  and  $\phi = 5\pi/4$ . Absolute value of  $u$ -velocity is almost the same for  $\phi = \pi/4$  and  $\phi = 3\pi/4$ , and is greater than for other  $\phi$  values.

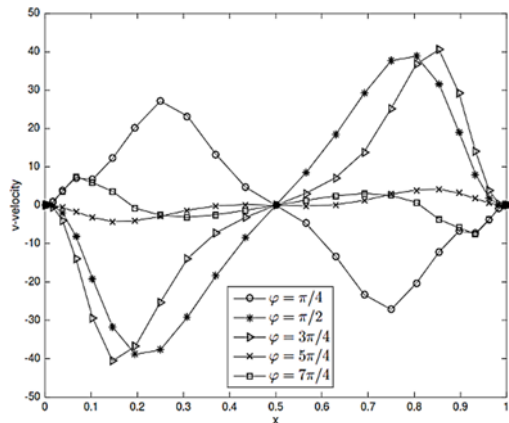
$v$ -velocity has a symmetric, almost sinusoidal behaviour at  $\phi = 5\pi/4$  and  $\phi = 7\pi/4$ . due to the counter rotating secondary cells in streamlines. Absolute value of  $v$ -velocity increases at a shorter  $x$ -value at  $\phi = 3\pi/4$  than  $\phi = \pi/4$  because of more rapid rising of heat in  $v$ -velocity direction at  $\phi = 3\pi/4$ . Similar rapid rising is also noticed at  $\phi = \pi/2$ .

In Fig. 4,  $\overline{Nu}$  is investigated as the angle  $\phi$  changes in different  $Ha$  values. Most of the change is noticed at  $Ha = 10$  ( $\theta = 0$ ). In this case, buoyancy force dominates over the applied magnetic field at a small  $Ha$  value. A symmetry is seen from  $\phi = 0$  to  $\phi = \pi$ .

Due to the buoyancy force over the rising heat,  $Nu$  decreases at  $\varphi = \pi/2$ . From  $\varphi = \pi$  to  $\varphi = 3\pi/2$ , a reduction is observed in  $Ha = 10$  and  $Ha = 50$ . Then,  $\overline{Nu}$  increases from  $\varphi = 3\pi/2$  to  $\varphi = 7\pi/4$  at only  $Ha = 10$ . For large  $Ha$  ( $Ha = 100$ ), the effect of  $\varphi$  on heat transfer almost disappears. This points to the retarding effect of the applied magnetic field on heat transfer. What's more,  $\varphi = 300^\circ = 5\pi/3$  and  $\varphi = 315^\circ = 7\pi/4$  can also be interpreted as  $\varphi = -60^\circ$  and  $\varphi = -45^\circ$ .



(a)  $u$ -velocity change



(b)  $v$ -velocity change

**Fig. 3. Velocity profiles along the line  $y = x$  with respect to  $\varphi$  when  $Ra=10^5, Ha = 10, \theta = 0$ .**

Figure 5 reveals the relation between  $\overline{Nu}$  and  $\varphi$  in various  $Ra$  values. No variation in  $\overline{Nu}$  for  $Ra=10^3$  indicates that heat transfer is not affected by  $\varphi$  at a small  $Ra$  value. As in Fig. 4 in the case of  $Ha = 10$ , the variation of  $\overline{Nu}$  at  $Ra=10^4 - 10^6$  is similar to each other. Only an increase in convective heat transfer is pronounced at  $Ra \geq 10^4$  at  $\varphi = -60^\circ$  and  $\varphi = -45^\circ$ . This may be due to the buoyancy force causing the rapid movement of the heated fluid when the enclosure took the rightly inclined position in which the heated wall becomes almost at the top.

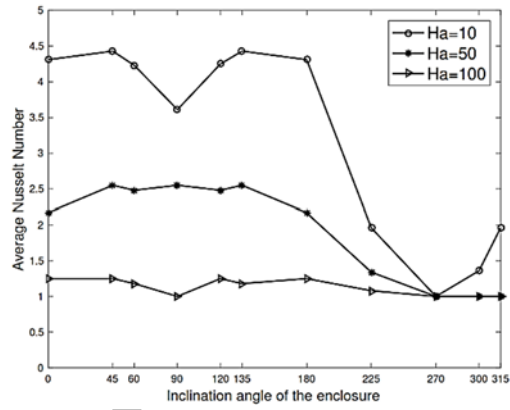


**Fig. 4.  $\overline{Nu}_h$  variation in different inclination angles  $\varphi$  of the cavity and in different  $Ha$  numbers when  $Ra=10^5, \theta = 0$ .**

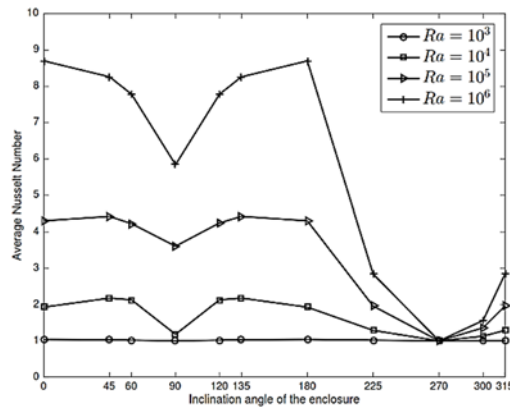


**Fig. 5.  $\overline{Nu}_h$  variation in different inclination angles  $\varphi$  of the cavity and in different  $Ra$  numbers when  $Ha = 10, \theta = 0$ .**

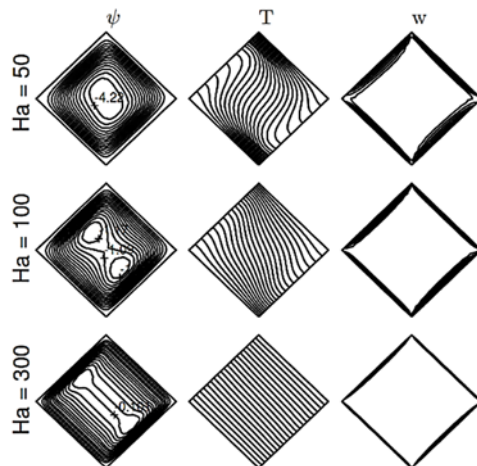


**Fig. 6. Hartmann number variation with  $Ra = 10^5, \varphi = \pi/4, \theta = 0$ .**

The Lorentz force inhibits the heat transfer and also fluid flow. This is well observed at  $Ha = 300$  in Fig. 6. Centered cell in streamlines is divided into secondary cells at  $Ha = 100$ . Then, a strong

clustering of streamlines through the heated and cold walls, and a reduction in fluid velocity (as is seen in marked contour values in streamlines) are emphasized at  $Ha = 300$ . For  $Ha = 300$ ,  $31 \times 31$  grids with  $\Delta t = 0.001$ ,  $\gamma = 0.01$  and  $c = 0.032$  have been used. Almost stationary behaviour in vorticity contours is also noted due to decrease in fluid motion.

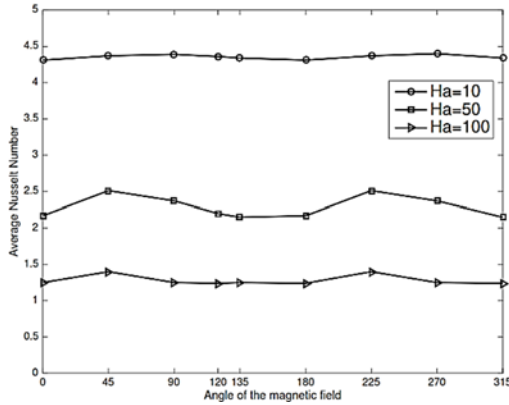


**Fig. 7.** Average Nusselt number variation in different angles  $\theta$  of applied magnetic field and in different  $Ha$  numbers when  $Ra=10^5$ ,  $\phi = 0$ .

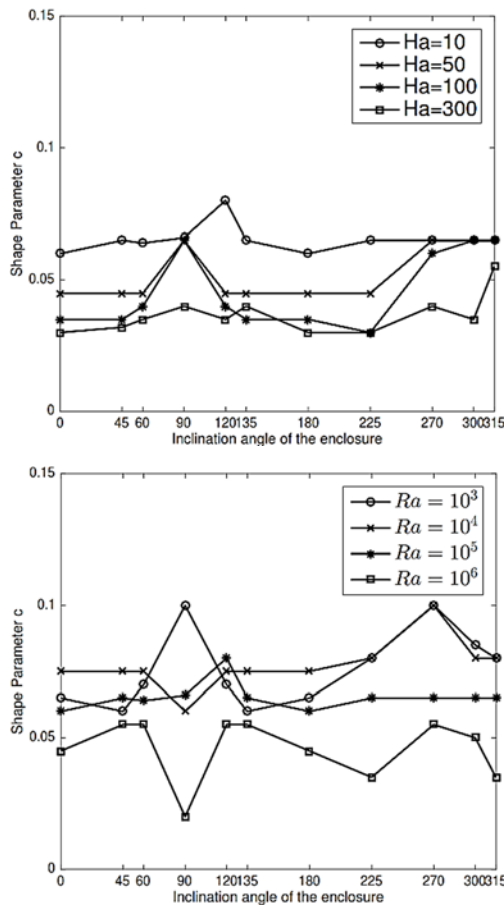


**Fig. 8.** Shape parameter variation in different  $\phi$  with different  $Ha$  and  $Ra$  values.

The impact of the angle of the applied magnetic field on  $\overline{Nu}$  is represented in Fig. 7. No much alteration

is seen in  $\overline{Nu}$  in each  $Ha$  values. Only a small peak is noticed at the angles  $\phi=\pi/4$  and  $\phi=5\pi/4$  for  $Ha = 50$  and  $Ha = 100$  which points to a small increase in convective heat transfer. Regardless of  $\phi$ , conductive heat transfer arises as  $Ha$  increases.

In Fig. 8 and Fig. 9, the influence of inclination angle  $\phi$  on the shape parameter  $c$  in various values of  $Ha$  and  $Ra$  values is illustrated.  $c$  values for any  $Ha$  value when  $Ra=10^5$ ,  $\theta = 0$  in Fig. 8 are very close to each other, small changes are seen in  $c$  values. Also, for a very large  $Ha$  ( $Ha = 300$ ),  $c$  values are smaller than the  $c$  values for other  $Ha$  values. Notable oscillations in  $c$  values occur in different  $Ra$  values when  $Ha = 10$ ,  $\theta = 0$ .

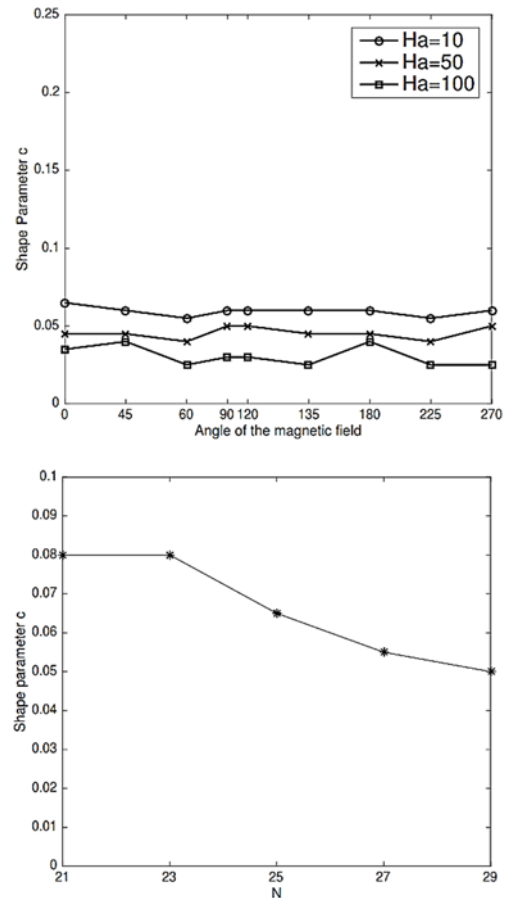


**Fig. 9.** Shape parameter variation in different  $\theta$  with different  $Ha$ , and  $N$  values.

Shape parameter  $c$  almost take the same values in different angles  $\theta$  and  $Ha$ . As  $Ha$  increases,  $c$  decreases for all angles  $\theta$  as can be seen in Fig. 9 with  $Ra=10^5$ ,  $\phi = 0$ . Moreover, the increase in the number of grid points causes  $c$  to be reduced in which  $Ra=10^5$ ,  $Ha = 10$ ,  $\theta = 0$ ,  $\phi=\pi/4$  are performed.

### 5. CONCLUSION

The efficiency of RBF-DQ method in a concise ex-

planation is presented simulating the natural convective heat transfer in presence of an applied magnetic field and in a differentially heated tilted cavity. The values of average Nusselt number are in well agreement with the benchmark results performing the small number of grid points. The effect of inclination angle of the enclosure is noted at small values of Hartmann numbers, and Rayleigh numbers greater than  $10^4$ . Convective heat transfer is much pronounced at  $\varphi = 0 - \pi$  than  $\varphi = 5\pi/4 - 7\pi/4$ .

## REFERENCES

- Basak, T., A. K. Singh, T. P. Akshaya Sruthi and S. Roy, (2014). Finite element simulations on heat flow visualization and entropy generation during natural convection in inclined square cavities. *International Communications in Heat and Mass Transfer* 51, 1–8.
- Bellman, R., B. G. Kashef and J. Casti (1972). Differential quadrature: a technique for a rapid solution of nonlinear partial differential equations. *Journal of Computational Physics* 10, 40–52.
- Brinkman, H. C. (1952). The viscosity of concentrated suspensions and solutions. *Journal of Chemical Physics* 20, 571–581.
- Buhmann, M. D. (2003). *Radial Basis Functions: Theory and Implementations*. Cambridge University Press.
- Cianfrini, C., M. Corcione and P. P. Dell’Omo (2005). Natural convection in tilted square cavities with differentially heated opposite walls. *International Journal of Thermal Sciences* 44, 441–451.
- Das, M. K. and K. S. K. Reddy (2006). Conjugate natural convection heat transfer in an inclined square cavity containing a conducting block. *International Journal of Heat and Mass Transfer* 49, 2987–5000.
- de vahl Davis, G. (1983). Natural convection of air in a square cavity: a bench mark numerical solution. *International Journal for Numerical Methods in Fluids* 3, 249–264.
- definite functions. *Constructive Approximation* 2, 1–12.
- Fasshauer, G. (2007). *Meshfree Approximation Methods with Matlab*. World Scientific Publications, Singapore.
- Franke, R. (1982). Scattered data interpolation: tests of some methods. *Mathematics of Computation* 38, 181–200.
- Han, C.Y. (2009). Effect of a magnetic field on natural convection of an electrically conducting fluid in a tilted cavity. *Journal of the Korean Physical Society* 55, 2193–2199.
- Huelsz, G. and R. Rechtman (2013). Heat transfer due to natural convection in an inclined square cavity using the lattice Boltzmann equation method. *International Journal of Thermal Sciences* 65, 111–119.
- Khanafer, K. M. and A. J. Chamkha (1999). Mixed convection flow in a lid-driven enclosure filled with a fluid-saturated porous medium. *International Journal Heat Mass Transfer* 42, 2465–2481.
- Kherief, N. M., F. Berrahil and K. Talvi (2016). Magneto-Hydrodynamic flow in a two-dimensional inclined rectangular enclosure heated and cooled on adjacent walls. *Journal of Applied Fluid Mechanics* 9, 205–213.
- Kherief, N. M., K. Talbi, F. Berrahil (2012). Effects of inclination and magnetic field on natural convection flow induced by a vertical temperature. *Journal of Applied Fluid Mechanics* 5, 113–120.
- Lacerda, C. R., M. J. Colaco (2014). Radial basis function applied to the solution of MHD flow in a tilted cavity. *Computational Thermal Sciences* 6, 461–476.
- Lo, D. C., D. L. Young, K. Murugesan, C. C. Tsai and M. H. Gou (2007). Velocity-vorticity formulation for 3D natural convection in an inclined cavity by DQ method. *International Journal of Heat Mass Transfer* 50, 479–491.
- Madych, W. R. and S. A. Nelson (1992). Bounds on multivariate polynomials and exponential error estimates for multiquadric interpolation. *Journal of Approximation Theory* 70, 94–114.
- Michelli, C. A. (1986). Interpolation of scattered data: Distance matrices and conditionally positive
- Munir, F. A., N. A. C. Sidik and N. I. N. Ibrahim (2011). Numerical simulation of natural convection in an inclined square cavity. *Journal of Applied Sciences* 11, 373–378.
- Pirmohammadi, M. and M. Ghassemi, M. (2002). Effect of magnetic field on convection heat transfer inside a tilted square enclosure. *International Communications of Heat Mass Transfer* 9, 3–42.
- Ravnik, J., L. Skerget and Z. Zunic (2008). Velocity-vorticity formulation for 3D natural convection in an inclined enclosure by BEM. *International Journal of Heat Mass Transfer* 51, 4517–4527.
- Shu, C. (2000). *Differential Quadrature and Its Application in Engineering*. Springer, London.
- Shu, C. and Y. L. Wu (2007). Integrated radial basis functions-based differential quadrature method and its performance. *International Journal of Numerical Methods in Fluids* 53, 969–984.
- Shu, C., H. Ding, H. Q. Chen and T. G. Wang (2005). An upwind local RBF-DQ method for simulation of inviscid compressible flows. *Computer Methods in Applied Mechanics and Engineering* 194, 2001–2017.

B. Pekmen Geridönmez / *JAFM*, Vol. 10, No. 2, pp. 499-507, 2017.

Shu, C., H. Ding, K. S. Yeo (2004). Solution of partial differential equations by a global radial basis function-based differential quadrature method. *Engineering Analysis with Boundary Elements* 28, 1217–1226.

Trefethen, L. N. (2000). *Spectral Methods in Matlab*.

SIAM, Philadelphia.

Williamson, N., S. W. Armfield, W. Lin and M. P. Kirkpatrick (2016). Stability and Nusselt number scaling for inclined differentially heated cavity flow. *International Journal of Heat and Mass Transfer* 97. 787–793.